INTERNATIONAL COMMUNICATIONS IN HEAT AND MASS TRANSFER

https://www.journals.elsevier.com/international-communications-in-heat-and-mass-transfer

Impact factor = 5.683

Accepted March 25th 2022

THERMO-SOLUTAL DUAL STRATIFIED CONVECTIVE MAGNETIZED FLUID FLOW FROM AN EXPONENTIALLY STRETCHING RIGA PLATE SENSOR SURFACE WITH THERMOPHORESIS

MD. Shamshuddin[1*], F. Mabood[2], Govind. R. Rajput[3], O. Anwar Bég[4], I.A. Badruudin[5]

*[1]Department of Mathematics, Vaagdevi College of Engineering (Autonomous), Bollikunta, Warangal, Telangana, **India**.*
**Corresponding author- Email: shammaths@gmail.com*
*[2]Department of Information Technology, Fanshawe College London, ON, **Canada**.*
Email: mabood1971@yahoo.com
*[3]Department of Applied Sciences and Humanities, SVKM's, NMIMS, Mukesh Patel School of Technology Management and Engineering, Shirpur campus, Shirpur-425405, **India.***
***Email:** g.rajput7@gmail.com*
*[4] Professor of Engineering Science & Director- Multi-Physical Engineering Sciences Group, Mechanical Engineering Department, School of Science, Engineering and Environment (SEE), University of Salford, Manchester, M54WT, **UK**.*
Email: O.A.Beg@salford.ac.uk
*[5]Department of Mechanical Engineering, College of Engineering, King Khalid University Asir - Abha 61421, **KSA.***
Email: magami.irfan@gmail.com

ABSTRACT

A theoretical study is presented for the coupled thermo-solutal free convection two-dimensional boundary layer flow of a of a magnetized fluid from an exponentially stretched magnetic sensor (Riga plate) surface. Heat generation/absorption, nonlinear thermal radiation and thermophoretic body force effects are included. Furthermore, thermal and solutal stratification are also featured in the boundary layer model. The derived nonlinear partial differential equation system with associated wall (sensor surface) and free stream boundary conditions is transformed to system of ordinary differential equations (ODE) via applicable similarity variables. A numerical solution is developed with the efficient Runge–Kutta–Fehlberg (RKF) technique with a shooting numerical method, in MATLAB software using the RKF-45 method. The graphical profiles were represented to examine the impacts of physically parameterics on the important physical stream features. Streamline and isotherm plots are also included for thermal buoyancy effect (Grashof number).Validation of solutions with earlier

simpler models is included. A relatively well agreement is achived between model prediction and the benchmark value. Values for skin friction factor, Nusselt number and Sherwood numbers are also tabulated to quantify momentum, heat and mass (species) transfer characteristics at the sensor surface. The results indicate that the significant depletion in temperature accompanies accumulation in magnetization and thermal stratification parameters. Significant accumulation in mixed convection and Riga plate electrode width parameter enhance the concatenation profiles. Nusselt number grows substantially as thermal stratification and radiative parameter increases. Sherwood number grows substantially as solutal stratification, thermophoresis and Schmidt parameter increases. The present study generalizes previous models to include *simultaneously* exponential stretching, thermophoresis, thermal and solutal (mass) stratification and heat source/sink effects.

KEYWORDS: *Magnetohydrodynamics (MHD); Riga sensor; Thermal radiation; Heat source/sink Thermal stratification; Solutal stratification; Thermophoresis; Boundary layers.*

1. INTRODUCTION

Electromagnetic sensors are complex, precision-engineered actuator devices which enable monitoring and measurement of delicate processes in numerous technologies including smart energy grids [2], surface crack detection in materials fabrication [3], bio-microfluidics [4], flexible electronics [5], earthquake disaster monitoring [6], naval drag control, electromechanical devices, robotics etc. They offer many advantages to conventional sensor systems including better operational ranges and tunable responsivity, isolation between components, and robust performance under intense loading and durable deployment in hazardous applications [4]. Many types of such sensors have been developed which exploit different magnetic phenomena including ferrofluid sensors [7], (which use a ferrofluid mass to convert the flow rate into quantifiable mass displacement), electromagnetic traps [8], Hall-sensors [9], magneto-resistive sensors [10], hybrid polymer foil magnetic micro-sensors [11]. An alternative system known as the Riga plate [12] was developed to exploit a wall-parallel Lorentz force and comprises a system of permanent magnets arranged with a series of aligned spanwise alternating electrodes. This electromagnetic actuator has been originally designed for skin friction and pressure drag minimization in hydronautics but has more recently been utilized in biomedical and other technical applications (e.g. submarines [13]). The design of Riga plate magnetic sensors involves a combination of fluid mechanics, electromagnetics and also heat and mass transfer. In mathematical models, to achieve robust flow control, crossed

electric and magnetic fields are applied to generate the wall-parallel Lorentz force and this permits modification of the boundary layer flow, pressure gradient etc. Boundary layer control is achieved with regulation of the electrical and magnetic field strengths. The rich arena of multi-physical transport phenomena inherent to Riga plate sensor flows has stimulated considerable interest in mathematical modelling, which provides an important compliment to experimental testing. These studies have considered different working fluids and also a wide range of thermophysical effects. Ganesh *et al.* [14] studied the transient squeezing dynamics of non-Newtonian (tangent hyperbolic) liquid in a Riga sensor with thermal conductivity variation. Islam *et al.* [15] used MATLAB explicit finite difference routines to compute the magnetized flow along a rotating Riga plate, presenting solutions for primary velocity, secondary velocity, temperature, local shear stress and Nusselt number. Loganathan and Deepa [16] presented numerical solutions for the effects of chemical reaction and heat source/sink on viscoplastic magnetized flow along a permeable Riga-plate. They noted increment in modified Hartmann number and heat generation accelerates the flow. Ahmad *et al.* [17] used a perturbation technique to study the mixed convection boundary layer flow of a nanofluid past a vertical porous Riga plate with strong suction, using a Grinberg-term for the wall parallel Lorentz force. Further studies include Ahmad *et al.* [18] (on nanofluid transport from Riga plate) and Ramesh *et al.* [19] (who considered viscoelastic convective nanofluid flow from a Riga sensor surface). These investigations all confirmed the considerable manipulation possible with magnetic forces in boundary layer characteristics on a magnetic Riga sensor. In numerous biomedical and emerging energy applications, *high temperatures* may arise which invoke radiative heat transfer in addition to conduction and convection heat transfer [20]. These include biotechnological radiation pumps [21], metamaterial devices [22], thermophotovoltaic fuel cells [23], hyperthermia treatments [24]. Mass transfer is also featured in numerous medical applications such as aerosolized drug delivery [25-26] and intraperitoneal drug delivery [27]. In many of these processes, magnetic sensors may be deployed. Although many approaches are available for simulating thermal radiation effects including photon transport models, Monte Carlo simulation and discrete ordinates models, a simpler methodology is the use of an algebraic flux model which avoids the need to solve the full radiative heat transfer equation. Several works have explored therefore the impact of thermal radiation in Riga plate electromagnetic fluid dynamics using a flux model, of which the Rosseland diffusion model is the most popular. Rosseland's model is generally valid for optically thick fluids and considers absorption but not scattering effects. It is very suitable for implementation in boundary layer flows. Ramzan *et al.* [28] examined the combined influence of effects of chemical reaction and

Rosseland radiative flux on viscoelastic nanofluid flow from a variable thickness convectively heated Riga plate with wall slip and zero mass flux conditions. Mishra *et al.* [29] used the variational parameter method (VPM) to compute the effects of thermal relaxation, thermal radiation, viscous heating and Ohmic dissipation in electromagnetic squeezing thermo-solutal flow between Riga plate sensors. They presented extensive solutions for velocity, temperature, concentration distributions and also reduced skin friction, Nusselt number and Sherwood number, observing a strong elevation in temperature with radiative effects. Rooman *et al.* [30] implemented a homotopy analysis method (HAM) to simulate the collective effects of Rosseland radiative flux, variable thermal conductivity and chemical reaction on entropy generation in magnetized. Williamson rheological nanofluid flow from a vertical Riga sensor plate. They noted that stronger magnetic field accelerates the flow whereas elevation in radiative flux intensity and temperature ratio parameter enhance entropy generation (Bejan number). Shafiq *et al.* [31] used the optimal homotopy analysis method (OHAM) coded in BVPh2.0 in MATLAB, to study the radiative-convective stagnation point flow of Walters-B viscoelastic magnetic flow along a Riga plate with Newtonian heating. They observed a strong enhancement in temperatures and a decrease in Nusselt number at the sensor surface with stronger radiative flux. Additional studies include Zainal et al. [32] (on radiative hybrid nanofluid magnetized Hiemenz stagnation flow from a porous contracting/expanding Riga plate) and Rawat *et al.* [33] (on radiative convective copper/silver-aqueous nanofluid boundary layer flow from a vertical Riga sensor surface).

In many magnetic sensor systems (and other applications including optical fiber and semiconductor wafer fabrication), *micro-particle* transport due to a temperature gradient may arise. This temperature gradient generates a net force on particles arising from a disparity in forces due to molecular collisions from the hotter and colder regions in the fluid. This effect is known as *thermophoresis* [34] and is important in aerosols, magnetic fluids, high temperature radiative systems etc. It leads to the deposition of small micron sized particles on cold surfaces and the repulsion of particles from hotter regions (or surfaces) with a particle-free layer arising in the vicinity of hotter surfaces bodies [35-36]. A number of investigations of thermophoretic effects in both non-magnetic and magnetohydrodynamics (MHD) boundary layer flows have been reported in recent years. These include Ganesan *et al.* [37] who considered free convection. Das *et al.* [38] used a shooting numerical method to analyse MHD slip from with wall transpiration and variable viscosity and thermal conductivity. They noted that concentration is depleted with greater thermophoretic body force. Zueco *et al.* [39] deployed an electrothermal network simulation code (PSPICE) to study the combined effects of Joule

heating and thermophoresis on magnetized boundary layer convection flow from a porous wall. They observed that mass diffusion to the wall is enhanced with thermophoresis whereas concentration boundary layer thickness is reduced. Several articles have also addressed thermophoresis effects in Riga plate sensor boundary layer flow. Madhukesh *et al.* [40] used a Runge–Kutta–Fehlberg 45 shooting scheme to compute the thermophoretic magnetic nanofluid flow from a Riga sensor wall with Newtonian heating. They noted an increment in velocity with modified Hartmann (magnetic) number and a boost in concentration magnitudes with Schmidt number. However, a strong depletion in concentration was observed with increasing thermophoretic parameter. Abo-Elkhair *et al.* [41] used semi analytic solutions for magnetic force effects acting on peristaltic transport of hybrid bio-nanofluid. Madhukesh *et al.* [42] also investigated the laminar, steady thermophoretic viscoplastic (Casson) hybrid magnetized nanofluid boundary layer flow from a Riga plate surface adjacent to a porous medium. Fatunmbi *et al.* [43] presented power series homotopy and Galerkin weighted residual method solutions for entropy generation in reactive non-Newtonian dissipative nanofluid MHD flow from a permeable vertical Riga surface embedded in a porous medium with radiative, thermophoresis and variable thermal conductivity effects. They showed that temperature and thermal boundary layer thickness are elevated with thermophoretic parameter whereas the flow is accelerated with increasing magnetic field strength. They also observed an elevation in entropy generation (Bejan number) with Biot and Eckert numbers and a decrease with porous media (Darcy) parameter.

The above studies generally considered a *stagnant* (stationary) sensor surface or a *linear* stretching surface. However more complex stretching dynamics may arise where the surface is extended quadratically or exponentially which permits more sophisticated manipulation of the wall transport characteristics. Several researchers have considered flows from *exponential* stretching surfaces. Bég *et al.* [44] used an explicit finite difference method to compute the transient MHD mixed convective boundary layer flow of a nanofluid from an exponentially stretching sheet in porous media. They noted that exponential stretching velocity strongly modifies the momentum and thermal characteristics and that temperature and nanoparticle concentration are significantly modified with thermophoresis effect and strongly boosted with elapse in time. Partha *et al.* [45] studied the mixed convective Newtonian dissipative flow from an exponentially stretching vertical surface. They highlighted the strong modification in transport characteristics for both aiding and opposing flow buoyancy cases and a morphing in velocity and temperature with Gebhart number and exponential stretching velocity. Further works on exponential stretching surface flows include Akbar *et al.* [46] (for magnetic

nanofluids), Shamshuddin *et al.* [47] and Sajid and Hayat [48] (on radiative-convective non-Newtonian magnetic slip flows with Hall current and Joule heating) and Bidin and Nazar [49] (on radiative heat transfer in convective boundary layers).

The above studies did not simultaneously consider exponential stretching and thermophoresis for the case of a Riga plate. In the present article we therefore examine the incompressible stead-state two-dimensional thermo-solutal free convective magnetized boundary layer fluid flow from an exponentially stretched magnetic sensor (Riga Plate) surface. The novelty of the current study is that effects of heat generation/absorption, nonlinear thermal radiation and thermophoretic body force are included. Furthermore, thermal and solutal stratification are also incorporated [50-51] which have also been neglected thus far in Riga plate electromagnetic actuator flows. A numerical solution is developed using a Runge–Kutta–Fehlberg (RKF) with shooting [52] for the transformed conservation equations under physically appropriate wall (sensor surface) and free stream conditions. *The present study therefore generalizes previous Riga plate mathematical models to include simultaneously exponential stretching, thermophoresis, thermal and solutal (mass) stratification and heat source/sink effects.* Extensive visualization of the influence of emerging parameters such as thermal Grashof number, magnetic interaction number, electrode parameter, thermal radiation parameter, heat source/sink parameter, Schmidt number, thermal and solutal stratification parameters and thermophoretic parameter on velocity, temperature, concentration are presented. Streamline and isotherm plots are also included for thermal buoyancy effect (Grashof number).Validation of solutions with earlier simpler models is included. Values for skin friction factor, Nusselt number and Sherwood numbers are also plotted to quantify momentum, heat and mass (species) transfer characteristics at the sensor surface.

2. MATHEMATICAL MODEL

The two-dimensional steady-state, incompressible, free convective magnetized fluid flow from an exponentially stretched Riga plate electromagnetic actuator sensor surface with heat and mass transfer is considered in an (x, y) coordinate system, as shown in Fig. 1.

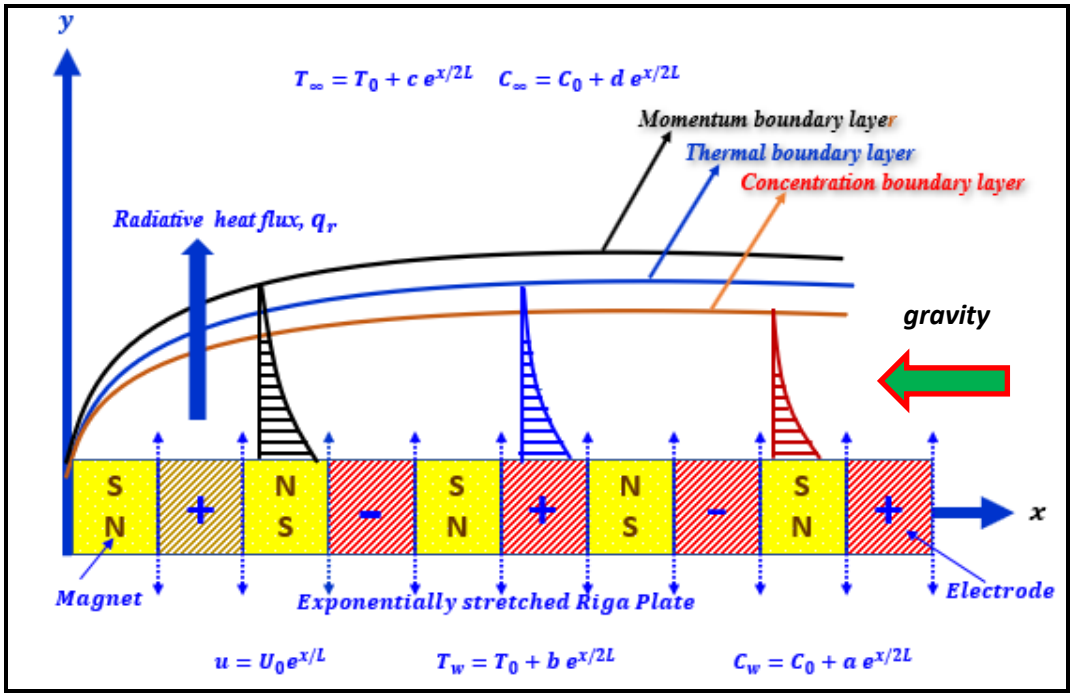

Figure 1. Geometry of the exponentially stretched Riga plate surface

The effects of heat source/sink, thermal radiation and thermophoresis are included. Thermal and solutal (mass) stratification are also considered. Hall current is neglected. The Riga plate is orientated in the *x*-direction. Gravity is also in the *x*-direction so that the Riga plate is actually *vertical*. The Riga plate has magnetization $M = M_0 x$ at $y = 0$, with uniform temperature and concentration at the surface T_w, C_w which exceed the ambient temperature and concentration T_∞, C_∞. The stretching velocity of the Riga plate along x-axis is $u = U_0 e^{x/L}$, where U_0 signifies a reference velocity. On the Riga plate surface, the thermophoresis produces mass deposition variation. Under the above approximations, amalgamating the models of Hayat *et al.* [53] and Supian *et al.* [54], the governing conservation boundary layer equations i. e. mass, momentum, energy (heat) and concentration (species) for the regime under consideration may be stated as:

$$\frac{\partial u}{\partial x} + \frac{\partial v}{\partial y} = 0, \tag{1}$$

$$u\frac{\partial u}{\partial x} + v\frac{\partial u}{\partial y} = \upsilon\frac{\partial^2 u}{\partial y^2} + g\beta_0\left(T - T_\infty\right) + \frac{\pi J_0 M_0}{8\rho}e^{\frac{-\pi}{a_1}y}, \tag{2}$$

$$u\frac{\partial T}{\partial x} + v\frac{\partial T}{\partial y} = \alpha\frac{\partial^2 T}{\partial y^2} - \frac{1}{\rho Cp}\frac{\partial q_r}{\partial y} + \frac{Q_0\left(T - T_\infty\right)}{\rho Cp}, \tag{3}$$

$$u\frac{\partial C}{\partial x} + v\frac{\partial C}{\partial y} = D_B\frac{\partial^2 C}{\partial y^2} - \frac{\partial}{\partial y}\left[V_T\left(C - C_\infty\right)\right], \tag{4}$$

The associated wall and free stream boundary conditions are:

$$\begin{aligned} &y=0: \quad u=U_0 e^{\frac{x}{L}},\ v=0,\ T=T_w=T_0+be^{\frac{x}{2L}},\quad C=C_w=C_0+ae^{\frac{x}{2L}},\\ &y\to\infty:\ u=0,\ v=0,\ T=T_\infty=T_0+ce^{\frac{x}{2L}}, C=C_\infty=C_0+de^{\frac{x}{2L}}. \end{aligned} \tag{5}$$

Here u and v represent velocity components in the *x, y* directions, respectively, kinematic viscosity is υ, fluid density is ρ, plate surface magnetization associated with the permanent magnets is M_0, current density applied to electrodes is j_0, thermal diffusivity is α, thermal expansion is β_0, specific heat capacity is C_p, internal heat source/sink is Q_0, and species mass (molecular) diffusivity is D_B. To simulate the thermal radiative flux in the energy Eqn. (3), the Rosseland approximation is deployed [28,29, 54] for which:

$$q_r=-\frac{4\sigma_1}{3k_1}\frac{\partial T^4}{\partial y}. \tag{6}$$

Here σ_1 designates Stefan-Boltzmann constant and k_1 represents the absorption factor. Expanding T^4 using Taylor series about T_∞ and neglecting terms of higher order, leads to $T^4\approx 4T_\infty^3T-3T_\infty^4$.

The thermophoretic term featured in the concentration boundary layer Eqn. (4)

Introducing V_T according to Alam *et al.* [55]:

$$V_T=\frac{-k_{th}\upsilon}{T_{ref}}\frac{\partial T}{\partial y}, \tag{7}$$

Here k^{th} denotes thermophoretic coefficient which is defined as:

$$k=\frac{2C_s\left(\lambda_g/\lambda_p+C_tK_n\right)\left[1+K_n\left(C_1+C_2e^{-\frac{C_3}{K_n}}\right)\right]}{\left(1+3C_mK_n\right)\left[1+2\lambda_g/\lambda_p+2C_tK_n\right]}, \tag{8}$$

Here the constant terms are C_1, C_2, C_3, C_t, C_s and C_m. λ_g, λ_p are the fluid thermal conductivities and K_n is Knudsen number. The thermophoretic parameter (τ) is defined by

$$\tau=-\frac{k\{T_w-T_\infty\}}{T_{ref}}. \tag{9}$$

Introducing a stream function $\psi(x)=\sqrt{2U_0\upsilon L}\ e^{x/2L}$ defined in terms the Cauchy-Riemann equations, $u=\partial\psi/\partial y$ and $v=-\partial\psi/\partial x$ Eqn. (1) is automatically satisfied. For simplification of

the current model, the following similarity transformations are utilized, following Hayat *et al.* [53]:

$$\eta=\sqrt{\frac{U_0}{2\upsilon L}}y\ e^{\frac{x}{2L}},\ u=U_0\ f'(\eta)e^{\frac{x}{L}},v=-\sqrt{\frac{\upsilon U_0}{2L}}\left[\eta\ f'(\eta)+f(\eta)\right]e^{\frac{x}{2L}},$$
$$\theta=\frac{T-T_\infty}{T_w-T_0},\ \ \phi=\frac{C-C_\infty}{C_w-C_0}. \tag{10}$$

Substitution of Eqn. (10) into Eqns. (2)-(4) leads to the dimensionless self-similar momentum, energy and concentration boundary layer Eqns.:

$$f'''+f\ f''-2f'^2+\lambda\,\theta+Q\,e^{-A\eta}=0, \tag{11}$$

$$\left(1+\frac{4R}{3}\right)\theta''+\Pr\left(f\theta'+S\theta-f'\theta-St.f'\right)=0, \tag{12}$$

$$\phi''+Sc\left[f\phi'-f'\phi-\tau\left(\phi\theta''+\phi'\theta'\right)-Sm.f'\right]=0, \tag{13}$$

The emerging transformed boundary conditions (5) assume the form:

$$f'(0)=1,\ f(0)=0,\ \theta(0)=1-St,\ \phi(0)=1-Sm,$$
$$f'(\infty)\to 0,\ \theta(\infty)\to 0,\ \phi(\infty)\to 0. \tag{14}$$

Here the primes refer to differentiation regard to similarity variable η and the following dimensionless parameters arise:

$$St=\frac{c}{b},\ Sm=\frac{d}{a},\ \lambda=\frac{2g\beta\left(T_w-T_0\right)L}{U_0^2e^{\frac{2x}{L}}},\ A=\frac{-\pi}{a}\sqrt{\frac{2\upsilon L}{U_0}}e^{\frac{2x}{L}},\ Q=\frac{\pi J_0M_0L}{4\rho U_0^2e^{\frac{2x}{L}}},$$
$$Sc=\frac{\upsilon}{D_B},\ S=\frac{2Q_0L}{\rho CpU_0e^{\frac{x}{L}}},\ R=\frac{4\sigma^*T_\infty^3}{kk^*},\ \Pr=\frac{\upsilon}{\alpha},\tau=\frac{-\left(T_w-T_0\right)k_{th}}{T_{ref}}. \tag{15}$$

In Eqn. (15), S_t, S_m denote thermal and solutal stratification parameters, λ is represented by thermal Grashof number, A indicates dimensionless parameter associated with the magnetic surface electrode width, Q indicates modified magnetic interaction number, Sc stands for Schmidt number, S indicates thermal heat source/sink parameter, R stands for thermal radiation parameter, $\Pr$ designates Prandtl number and τ symbolizes thermophoretic parameter. To compute momentum, heat and mass transfer characteristics at the exponentially elongated Riga sensor surface (wall), skin friction factor (non-dimensional shear stress), Nusselt number and Sherwood number can be expressed as:

$$C_f=\frac{\tau_w\big|_{y=0}}{\rho\,u_w^2},\quad Nu=-\frac{x\,q_w\big|_{y=0}}{k\left(T_w-T_\infty\right)},\quad Sh=-\frac{x\,q_m\big|_{y=0}}{D_B\left(C_w-C_\infty\right)}, \tag{16}$$

Here the *dimensional wall shear stress, thermal flux and solutal flux* take the form:

$$\tau_w = \mu \left.\frac{\partial u}{\partial y}\right|_{y=0}, \; q_w = -k\left(1+\frac{4R}{3}\right)\left.\frac{\partial T}{\partial y}\right|_{y=0}, \; q_m = -D_B \left.\frac{\partial C}{\partial y}\right|_{y=0}, \tag{17}$$

Invoking the non-dimensional transformations (10), the following relations emerge:

$$\begin{aligned}
&\sqrt{\frac{2L}{x}}\sqrt{\mathrm{Re}_x}\; C_f = f''(0), \\
&\sqrt{\frac{2L}{x}}\frac{Nu_x}{\sqrt{\mathrm{Re}_x}} = -\left(1+\frac{4R}{3}\right)\frac{1}{1-St}\theta'(0), \\
&\sqrt{\frac{2L}{x}}\frac{Sh_x}{\sqrt{\mathrm{Re}_x}} = -\frac{1}{1-Sm}\phi'(0).
\end{aligned} \tag{18}$$

Here $\mathrm{Re}_x = U_0\, e^{x/L}\, x/\upsilon$ indicates local Reynolds number.

3. NUMERICAL SOLUTION AND VALIDATION

The transformed ordinary differential boundary value problem defined by Eqns. (11)-(13) along with boundary conditions (14) are strongly nonlinear and coupled. A numerical solution is therefore sought using the fourth order Runge–Kutta–Fehlberg (RKF) with the shooting method. This method converts the equations to the set of IVPs (Initial Value Problems) with unknown initial conditions, which can be dealt with suitable guesses. In this present situation, we substituted the variables $p, q,\ r$ and s so that the collective 7th order system of equations (11)-(13) are transformed to *linear first order* differential equations (19)-(25) as:

$$f' = p, \tag{19}$$

$$p' = q, \tag{20}$$

$$q' = -fq + 2p^2 - \lambda r - Qe^{-A\eta}, \tag{21}$$

$$\theta' = r, \tag{22}$$

$$r' = \frac{-\mathrm{Pr}[rf + S\theta - p\theta - p\ St]}{\left(1+\frac{4R}{3}\right)}, \tag{23}$$

$$\phi' = s, \tag{24}$$

$$s' = -Sc\left[\, fs - p\phi - \tau\left(\phi r' + sr\right) - S\ p\,\right]. \tag{25}$$

The associated boundary conditions are:

$$f(0) = 0,\ p(0) = 1,\ \theta(0) = 1 - St,\ \phi(0) = 1 - Sm. \tag{26}$$

To solve equations (21), (23), (25) with (26) as an initial value problem the values of $q(0)$, $r(0)$ and $s(0)$ are needed. Since these values are not available, hence, the suitable guesses for $q(0)$, $r(0)$ and $s(0)$ are made and generated by the shooting scheme with other boundary conditions at $\eta \to \infty$. A step size of $\Delta\eta = 0.01$, is adopted, and an accuracy up to the fifth decimal place, is taken as the criterion of convergence.

3.1. Validation

To verify the RKF solution validity, we have extracted the reduced Nusselt number $-\theta'(0)$ values for various values of R and $\Pr$,and compared these with earlier solutions of Bidin & Nazar [49] and Mathur & Mishra [56]. The numerical outcomes are listed in **Table 1**. Evidently the solutions correlate very closely, and this confirms the accuracy of RKF approach.

Table 1: Comparison of $-\theta'(0)$ for different values of $\Pr$ and R when $\lambda = Q = S = St = 0$.

Pr	$R = 0$			$R = 0.5$		
	Bidin & Nazar [49]	Mathur & Mishra [56]	Present RKF results	Bidin & Nazar [49]	Mathur & Mishra [56]	Present RKF results
1	0.9548	0.9576	0.95478	0.6765	0.6936	0.67651
2	1.4714	1.4708	1.47146	1.0735	1.0744	1.07352
3	1.8691	1.8685	1.86907	1.3807	1.3802	1.38075

4. RESULTS AND DISCUSSION

Extensive computations have been conducted with the RKF method and shooting algorithm in MATLAB symbolic software. **Figs 2-5** illustrate the influence of selected parameters on velocity, temperature and concentration profiles. Additionally, streamline and isotherm contour plots are visualized in F**igs 6-7**. All data utilized is selected from [40], [42], [53], [54] and is physically representative of actual Riga plate actuator systems.

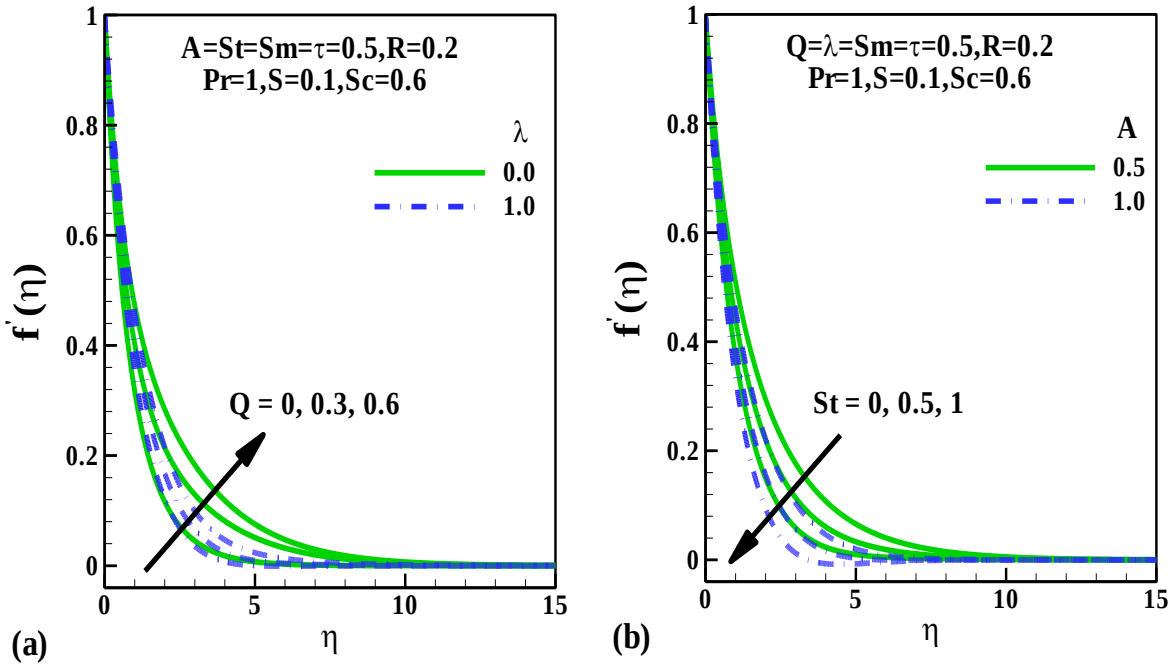

Fig. 2. Variation of velocity with (a) Q and λ (b) St and A

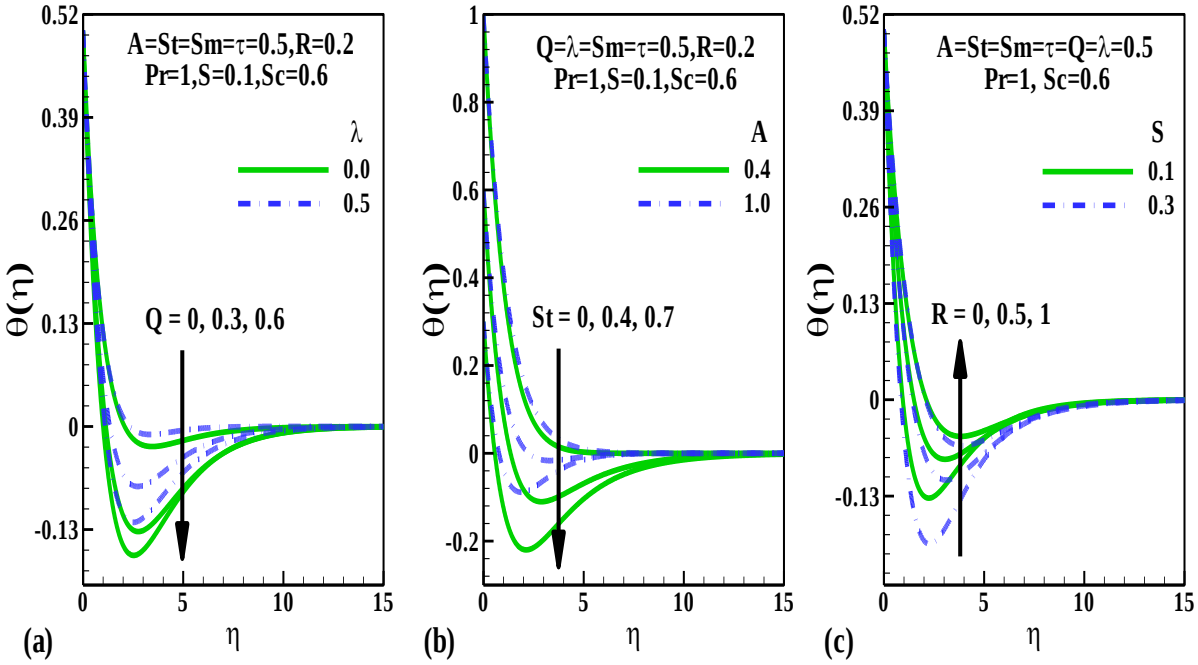

Fig. 3. Variation of temperatures with (a) Q and λ (b) St and A (c) R and S

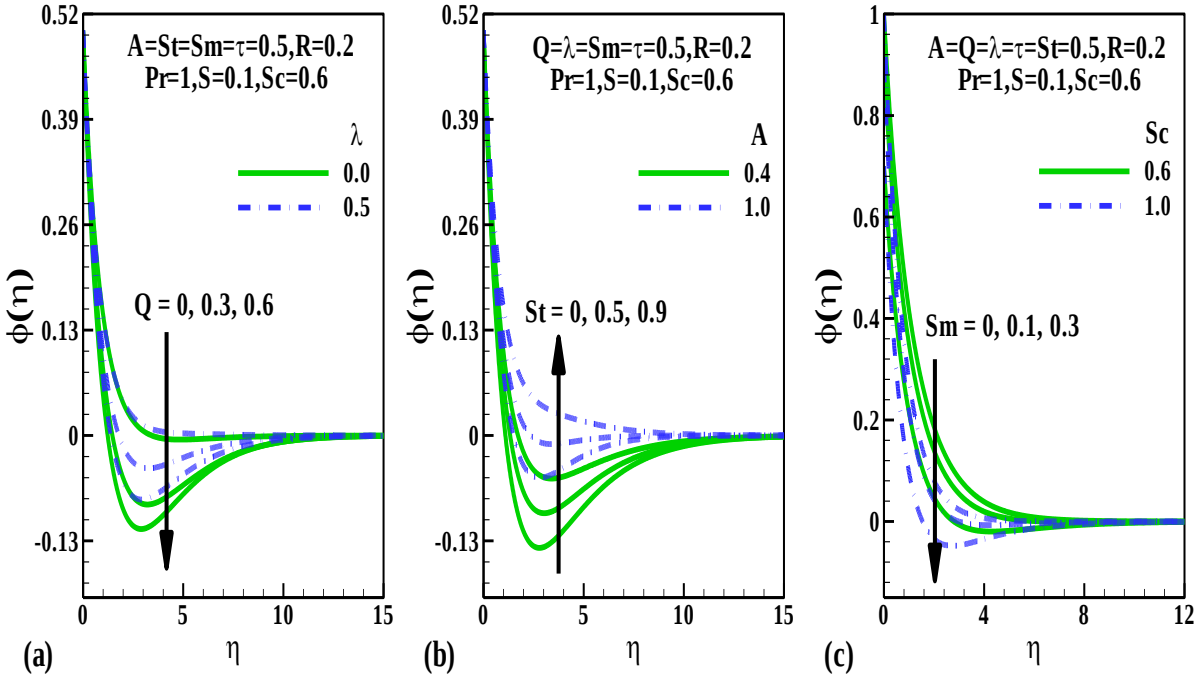

Fig. 4. Variation of concentration with (a) Q and λ (b) St and A (c) Sm and Sc

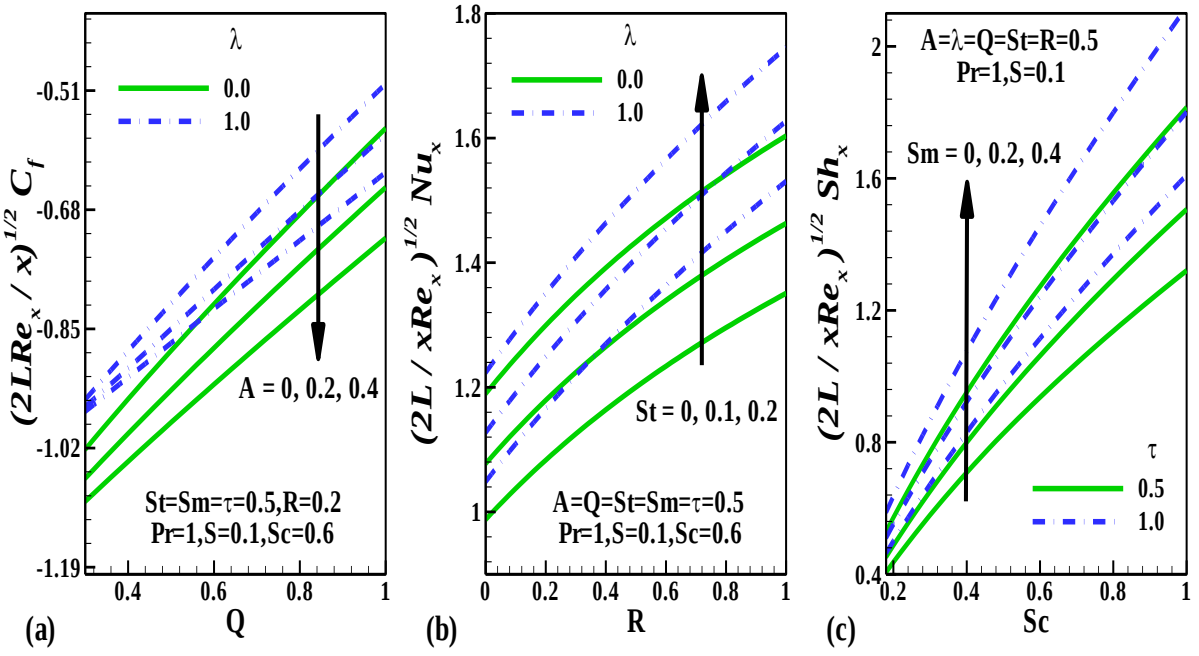

Fig. 5. Variation of (a) skin-friction distribution with Q and λ (b) Nusselt number distribution with St and R (c) Sherwood number distribution with Sm and Sc

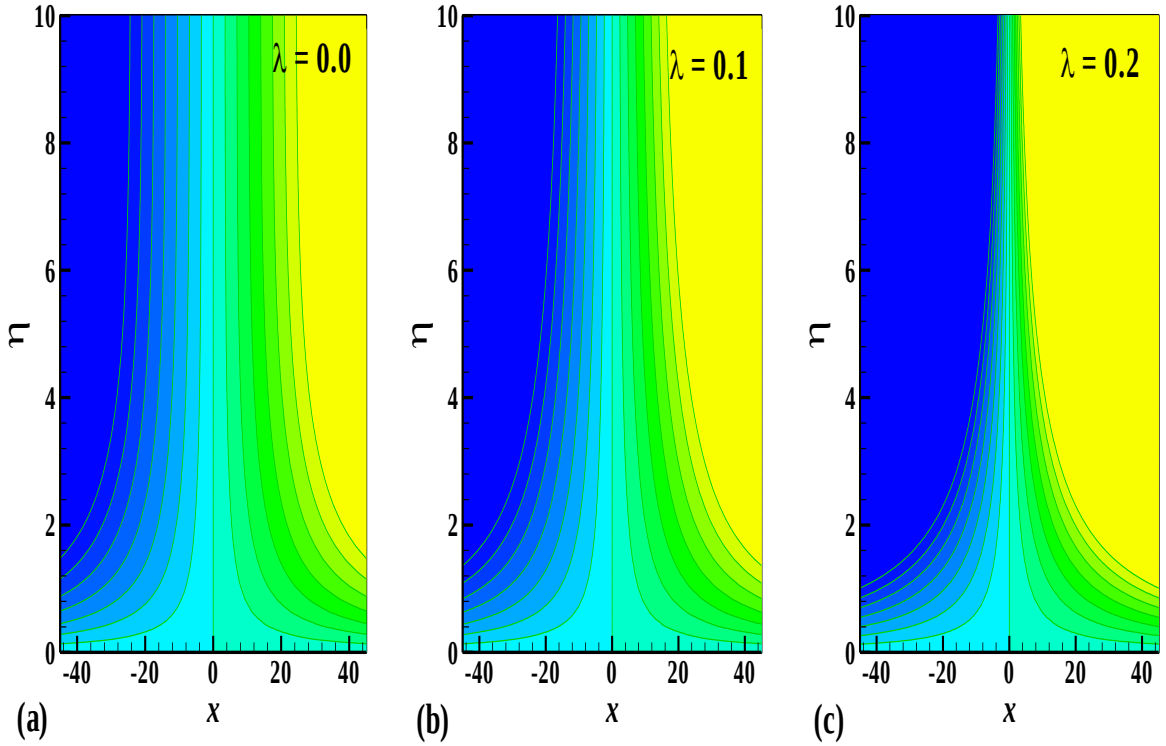

Fig. 6 Countour plots for streamlines with variation in λ

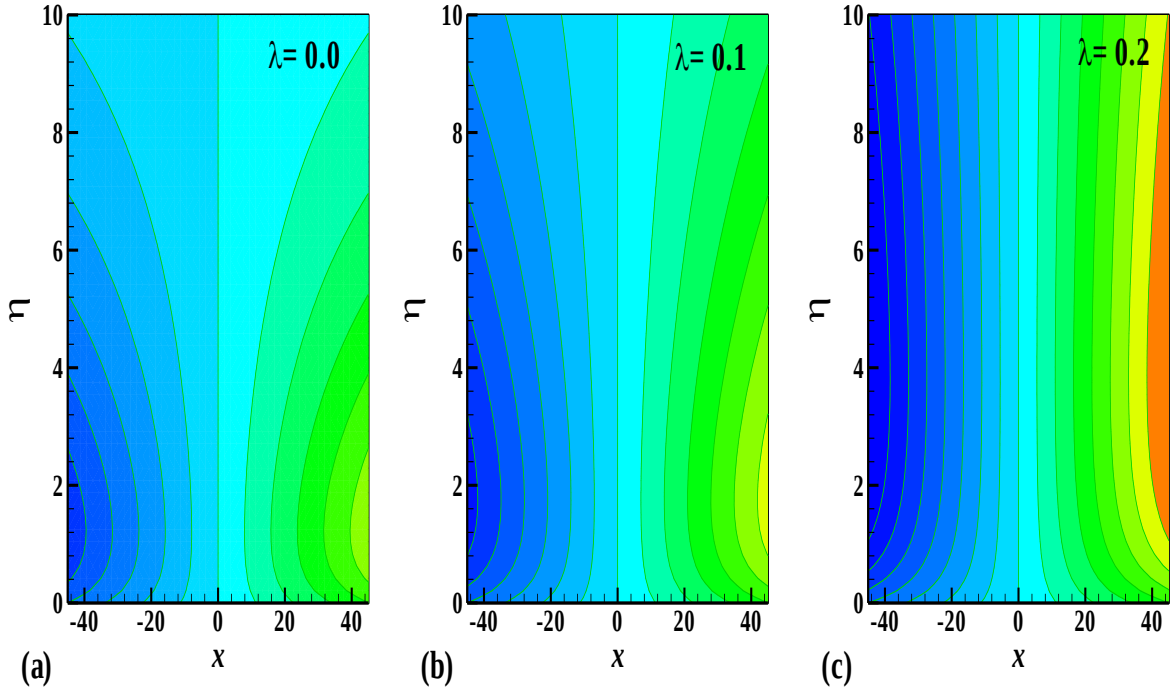

Fig. 7 Countour plots for isotherms with variation in λ

Fig. 2a shows the evolution in velocity through the boundary layer regime transverse to the sensor surface with increment in Q and λ. As Q is increased there is a strong elevation in velocity i.e. the flow is accelerated and the momentum boundary layer thickness is reduced. $Q = \pi J_0 M_0 L / 4\rho U_0^2 e^{2x/L}$ and is directly properitional to the magnitization in the Riga sensor surface. However the resulting magnetic body force is not retarding in nature, and is aligned with the sensor surface. This asssists momentum development and enhances velocities, a trend which is sustained at all $\eta-$values. Velocity is therefore minimized when magnetization vanishes i.e. $M_0 = 0$ and therefore $Q = 0$ for which momentum boundary layer thickness is a maximum. An increase in mixed convection parameter, λ, however induces the reverse effect to magnetic parameter. Higher values of λ damp the boundary layer flow and lead to a reduction in velocities. Thermal convection current therefore inihibit momentum development and decelerate the flow, causing an increase in momentum boundary layer thickness. The mixed convection parameter, $+\lambda\theta$ arises in the momentum Eqn. (11) and couples this equation to the energy (thermal boundary layer) eqn. (12). When $\lambda = 0$, these equations are decoupled and forced convection is present in the regime. This achieves the maximum velocity. Fig. 2b shows that with increasing thermal stratifcation parameter, St and greater magnetic and electrode width parameter, A, the velocity is significantly depleted. The parameter, $St = c/b$ and features in the term, $\Pr(-St\ f')$ in the energy Eqn. (12) and also the modified wall temperature boundary condition, $\theta(0) = 1 - St$ in Eqn. (14). Increment in St increases the inhibiitve force $\Pr(-St\ f')$ which opposes momentum development and decelerates the boundary layer flow. Momentum boundary layer thickness will however be increased. The case where thermal stratification is absent i.e. $St = 0$, achieves the maximum velocity and minimal momentum (hydrodynamic) boundary layer thickness. The parameter, $A = -\pi\sqrt{2\nu L / U_0}e^{2x/L} / a$ and arises in the exponent of the term, $+Q\,e^{-A\eta}$ in Eqn. (11). As A is increased, the electrode width is decreased, and the *overall assistive* term, $+Q\,e^{-A\eta}$, is decreased and this generates greater drag at the Riga plate surface. Momentum boundary layer thickness is therefore also enhanced. Clearly a substantial modification in velocity distribution is achieved with alteration in the electrode width parameter.

Fig. 3 illustrates the evolution in temperatures with (a) Q and λ (b) St and A (c) R and S. With increment in the magnetization parameter Q, as observed in Fig. 3a, there is a strong decrement in temperature, which descend very sharply from the sensor surface and

eventually reach the symptotically smooth convergent values in the freestream. Although Q does not feature in the energy eqn. (12), it is coupled to this eqn. via the mixed convective (thermal buoyancy) term, $+\lambda\theta$. Furthermore the momentum eqn. (11) is coupled to the energy eqn. (12) via the thermal convection terms, $\Pr\,(f\theta' - f'\theta)$ and the thermal stratification term, $\Pr\,(-St\ f')$.Temperature will therefore be substantially modified indirectly by magnetizationn effect. Thermal boundary layer thickness is suppressed in the regime with increasing Q. Conversely there is a marked elevation in temperature with enhancement in mixed convection parameter, λ. With greater values of this parameter the thermal buoyancy effect is accentuated and thermal diffusion is intensified. This heats the boundary layer and also boosts thermal boundary layer thickness. Fig. 3b shows that an increase in thermal stratification parameter, St significantly depresses temperature i.e. induces cooling, whereas the contrary effect is observed with elevation in the electrode width parameter, A. Thermal boundary layer thickness is therefore depleted with more intense thermal stratficaton since heat transfer is delaysed in the boundary layer, whereas thermal boundary layer thickness is boosted with electrode parameter elevation. Thermal diffusion in the boundary layer on the magnetic Riga sensor is therefore very sensitive to both stratification and electrode width changes. For the non-thermally stratified scenario, St = 0, temperatures are maximized. Fig 3c shows that a substantial enhancment in temperature is computed with increasing radiative parameter (R) whereas a reduction is observed with larger heat sink parameter, S. The thermal diffusion term is augmented with the radiative parameter, in the term, $\Pr\,(1+(4R/3))\theta''$ in the energy Eqn. (12). The intensification in radiative flux with greater R values energizes the boudnary layer which absorbs more thermal radiation releative to thermal conduction. When $R=0$, radiative effects vanish and only conduction and convection are present. Thermal boundary layer thickness is therefore much greater with radiative heat flux present than when it is absent. The increment in thermal sink effect with greater S value simplies increased releval of heat from the system. This cools the regime and decreases thermal boundary layer thickness.

Fig. 4 depicts the plots for concentration with transverse coordinate for (a) Q and λ (b) St and A (c) Sm and Sc**.** With an upsurge in Q (Fig. 4a) there is a significant plummet in the concentration (ϕ) magnitudes. Concentration (species) boundary layer thickness is therefore suppressed with stronger magnetization effect in the boundary layer along the sensor surface. Although magnetization parameter is absent in the species boundary layer Eqn. (13), this equation is strongly coupled to the momentum Eqn. (11) via the convective diffusion ters, $Sc(f\phi' - f'\phi)$ and solutal stratification terms, $Sc(-Sm\ f')$. An indirect efect is therefore

experienced in the solutal field with modification in magnetization parameter, *Q*. Increasing mixed convection parameter, λ (see Fig. 4b) also exerts an *indirect effect* on concentration via coupling with the energy Eqn. (12) through the thermophoresis terms, $-\tau(\phi\theta'' + \phi'\theta')$ in eqn. (13). Thermal buoyancy when altered in the momentum eqn. (11) influences the temperature field which cia coupling modifies the concentration distributions. While the flow is decelerated with greater thermal buoyancy, there is a weak elevation in concentration magnitudes. Mass diffusion is therefore encouraged with mixed convection effect and concentration boundary layer thickness is enhanced. An increase in thermal stratification parameter, *St*, also affects the concentration field via coupling between the thermal and species boundary layer eqns. While temperature is reduced with greater thermal stratification, the mass diffusion of species is assisted and particles disperse more effectively in the boundary layer. Concentration boundary layer thickness is therefore least for the case where there is no thermal stratification in the regime (*St* =0). An increase in electrode width parameter, $A = -\pi\sqrt{2\nu L / U_0}\, e^{2x/L} / a$ also considerably boosts the concentration magnitudes. Again the influence is indirect and due to coupling between the different conservation equations which enables the magnetic and electrode terms to exert an effect on mass transfer. Concentration elevation is in particular pronounced at intermediate distances from the sensor surface. Fig 4c shows that with an increment in Schmidt number, *Sc*, there is progressive reduction in concentration. Similarly larger values of solutal stratification parameter, *Sm*, also result in a significant depletion in concentration values. Schmidt number relates the momentum diffusivity to the molecular (solute) diffusitivity. For *Sc* = 0.6, the solutal diffusiion rate therefore exceeds the momentum diffusion rate (vorticity)which leads to higher values of concentration. However when *Sc* = 1 (oxygen difusing through aqueous solution) and the diffusion rates are the same (implying an equivalence in momentum and species boundary layer thicknesses), the mass diffusion is inhibited and there is a plummet in concentration magnitudes through the boundary later transverse to the magnetic Riga sensor surface. The solutal stratification parameter, *Sm* arises in the modified terms in the species conservation Eqn. (13), viz, $Sc(-Sm\ f')$ and also appears in the agmented wall concentration boundary condition (14), viz $\phi(0) = 1 - Sm$. Larger values of *Sm* imply a more disperse regime and particle diffusion (mass transfer) is inhibited. For the case *Sm* = 0, solutal stratification is negated and maximum concentration is observed with a corresponding maximum species boundary layer thickness on the magnetic sensor surface.

Fig 5 displays the distributions in (a) skin-friction with Q and λ (b) Nusselt number with St and R (c) Sherwood number with Sm and Sc. Fig 5a shows that with greater values

of mixed convection parameter, λ there is significant elevation in skin friction at the Riga plate surface. The profiles also grow linearly with increment in magnetization parameter, *Q*. However increment in electrode width parameter, *A*, leads to a depression in skin friction. The boundary layer flow is therefore accelerated at th Riga surface with stronger thermal buoyancy effect and greater magnetic field, whereas it is decelerated with greater electrode width effect. Fig. 5b shows that greater thermal stratification parameter, *St* and radiative parameter, *R*, both boost the Nusselt number, although at higher values of *R* the profiles become increasingly parabolic (nonlinear) in nature indicating a very strong modification in heat transfer to the plate surface with high radiative flux intensity. At lower values the profiles are approximately linear. An increment in mixed convection parameter λ significantly enhances Nusselt number magnitudes, since natural thermal convection currents intensify the heat transferred to the Riga plate surface. Fig. 5c illustrates that substantial enhancment in Sherwood number is induced with a rise in soutal stratification parameter, *Sm*, thermophoresis parameter, τ and also Schmidt number. Greater migration of particles under strong thermal gradient is encouraged with higher thermophoretic body force. The *mass transfer* to the wall is therefore elevated, as a result of the amplification in the terms, $Sc\left[-\tau(\phi\theta'' + \phi'\theta')\right]$ in the species boundary layer Eqn. (13). However since concentration values will be depeleted (greater species diffusion is produced towards the plate surface) in the boundary layer regime, the concentration boundary layer thickness will be suppressed with stronger thermophoretic effect. The reduction in concentration values with increment in Schmidt number (computed earlier) due to a reduction in molecular diffusivity, results in greater transport of particles via mass diffusion to the Riga sensor surface. This manifests in a boost in Sherwood numbers. Also the depeltion in cocentration values in the boundary layer regime with higher solutal stratification parameter (also computed earlier) produces an upsurge in particles migrating to the sensor surface, which effectively elevates the Sherwood number values at the Riga sensor plate wall.

Figs. 6 and 7 visualize the streamline and isotherm contour plots with a change in mixed convection parameter, with all other parameters constrained. Fig. 6 shows that with increasing λ values, the thermal buoyancy force is elevated and this causes an expansion in theright hand side yellow zone. However the streamlines in the central zone $(x = 0)$ are constricted and the blue zone $(-40 < x < 0)$ is intensified, indicating a strong deceleration in the regime with greater thermal buoyancy effect. The gradient in the streamlines at lower η values is also reduced and overall the left blue and right yellow zones are expanded laterally. There is also considerable contraction in the central zones especially at higher values of transverse

coordinate (η) which is absent for the forced convection case $(\lambda = 0)$. The flow on the Riga plate sensor surface is therefore strongly modiifed with amplification in thermal buoyancy (natural convection currents). Fig. 7 indicates that with increasing mixed convection parameter, $\lambda = 2g\beta\left(T_w - T_0\right)L / U_0^2 e^{2x/\mathrm{L}}$ the isotherms are progressively constricted (intensified) from the left zone to the right zone and morph from a parabolic topology to a vertical pattern especially in the core region (x ~0). A hotter (red) zone and also an adjacent warm yellow zone emerge at the extremity of the right zone (x = 40) and is present at all values of transverse coordinate, η. These hotter (yellow and red) regions are absent for the forced convection case $(\lambda = 0)$ and also the weaker mixed convection case $(\lambda = 0.1)$. With maximum thermal buoyancy effect $(\lambda = 0.2)$, the heat transfer is significantly intensified in the regime and temperatures are boosted mainly in the right zone but also elevated throughout the domain.

5. CONCLUDING REMARKS

A mathematical model has been developed for the coupled thermo-solutal free convection two-dimensional boundary layer flow of a of a magnetized fluid from an exponentially stretched magnetic sensor (Riga plate) surface. Heat generation/absorption, nonlinear thermal radiation and thermophoretic body force effects have been incorporated. Furthermore, thermal and solutal stratification are also studied. The dimensionless transformed ordinary differential boundary value problem is solved computationally with the efficient Runge–Kutta–Fehlberg (RKF) technique and a shooting algorithm, in MATLAB software. The impact of emerging parameters such as mixed convection parameter (thermal Grashof number), magnetic interaction number, electrode parameter, thermal radiation parameter, heat source/sink parameter, Schmidt number, thermal and solutal stratification parameters and thermophoretic parameter on velocity, temperature, concentration are visualized graphically. Streamline and isotherm plots are also included for thermal buoyancy effect (Grashof number).Validation of solutions with earlier simpler models is included. Values for skin friction factor, Nusselt number and Sherwood numbers are also tabulated to quantify momentum, heat and mass (species) transfer characteristics at the sensor surface. The main findings from the simulations may be summarized as follows:

- Velocity and momentum boundary layer thickness are respectively reduced and increased with increasing thermal stratification parameter, St and greater electrode width parameter, A.

- A significant depletion in temperature and thermal boundary layer thickness accompanies a rise in magnetization parameter *Q* and thermal stratification parameter, *St*.
- Incressing mixed convection parameter, λ, thermal stratification parameter, St, and Riga plate electrode width parameter, A, all enhance concentrations and species boundary layer thickness.
- Increasing thermal stratification parameter, *St* and radiative parameter, *R*, substantially enhance Nusselt number.
- A marked enhancment in Sherwood number is produced with an increment in soutal stratification parameter, *Sm*, thermophoresis parameter, τ and also Schmidt number.
- With increasing λ values, there is an expansion in the right zone, whereas the streamlines in the central zone $(x = 0)$ become increasingly constricted, indicating a strong deceleration in the regime with greater thermal buoyancy effect. Also a hotter (red) zone and warmer yellow zone are observed in the isotherm plots at the right extremity of the regime, which are not present for the forced convection case $(\lambda = 0)$ and also the weaker mixed convection case $(\lambda = 0.1)$.

The present investigation has revealed some interesting flow phenomena in Riga electromagnetic plate actuator boundary layer flows. However attention has been confiend to *Newtonian* fluids. Future studies may consider for example *Eringen's micropolar model for non-Newtonian effects* and will be communicated imminently.

REFERENCES

[1] J. Lenz, S. Edelstein, Magnetic sensors and their applications, IEEE Sensors J. 6 (2006) 631-649.

[2] Y. Ouyang, J. He, J. Hu, G. Zhao, Z. Wang, S.X. Wang, Contactless current sensors based on magnetic tunnel junction for smart grid applications, IEEE Trans. Magn. 51 (2015) 1-4.

[3] Z. Jin, M. Oogane, K. Fujiwara, Y. Ando, Magnetic sensor based on serial magnetic tunnel junctions for highly sensitive detection of surface cracks, J. Appl. Phys. 122 (2017) 174502. https://doi.org/10.1063/1.5001098.

[4] g. Lin, D. Makarov, O.G. Schmidt, Magnetic sensing platform technologies for biomedical applications, Lab Chip. 17 (2017) 1884–1912.

[5] M. Melzer, J.I. Monch, D. Makarov, Y. Zabila, G.S.C. Bermudez, D. Karnaushenko, S. Baunack, F. Bahr, C. Yan, M. Kaltenbrunner, O.G. Schmidt, Wearable magnetic field sensors for flexible electronics *Adv. Mater.* 27 (2015) 1274–1280.

[6] S. Yong, X. Wang, R. Pang, X. Jin, J. Zeng, C. Han, B. Xu, Development of inductive magnetic sensor for multi-component seismic monitoring system AETA. Acta Sci. Nat. Univ. Pekin. 54 (2018) 495-501.

[7] B. Andò, A. Ascia, S. Baglio, N. Savalli, A Novel Ferrofluidic Inclinometer, IEEE Transact. Instrumentation and Measurement. 56(4) (2007) 1114-1123.

[8] F. Li, J. Kosel, An efficient biosensor made of an electromagnetic trap and a magneto-resistive sensor Biosens. Bioelectron. 59 (2014) 145-150.

[9] M. Blagojevic, M. Kayal, M. Gervais, D. De Venuto, SOI Hall-sensor front end for energy measurement, IEEE Sensors J. 6 (2006) 1016– 1021.

[10] S. Tumanski, Thin Film Magnetoresistive Sensors, CRC Press, Florida, USA (2001).

[11] T. Griesbach, M.C. Wurz, L. Rissing, Design, fabrication, and testing of a modular magnetic field microsensor on a flexible polymer foil, IEEE Trans. Magn. 48 (2012) 3843-3846.

[12] A. Gailitis, O. Lielausis, On a possibility to reduce the hydrodynamic resistance of a plate in an electrolyte, Appl Magnetohydrodynamics Rep Phys Inst Riga, 12 (1961) 143-146

[13] V.V. Avilov, Electric and magnetic fields for the Riga plate, Technical Report, FRZ Rossendorf (1998).

[14] K. Ganesh Kumar, B.J. Gireesha, M.R. Krishnamurthy, N.G. Rudraswamy, An unsteady squeezed flow of a tangent hyperbolic fluid over a sensor surface in the presence of variable thermal conductivity, Results Phys. 7 (2017) 3031–3036.

[15] M.M. Islam, S. Khatun, M.T. Mollah, M.M. Alam, Fluid flow along the Riga plate with the influence of magnetic force in a rotating system, 8th BSME International Conference on Thermal Engineering, AIP Conf. Proc. 2121 (2019) 050002-1 - 050002-6. https://doi.org/10.1063/1.5115889

[16] P. Loganathan, K. Deepa, Stratified Casson Fluid Flow Past a Riga-plate with Generative/Destructive Heat Energy, Int. J. Appl. Comput. Math. 6 (2020) 113. https://doi.org/10.1007/s40819-020-00863-w

[17] A. Ahmad, S. Asghar, S. Afzal, Flow of nanofluid past a Riga plate. J. Magn. Magn. Mater. 402 (2016) 44–48.

[18] R. Ahmad, M. Mustafa, M. Turkyilmazoglu, Buoyancy effects on nanofluid flow past a convectively heated vertical Riga-plate: A numerical study. Int. J. Heat Mass Transf. 111 (2017) 827–835.

[19] G.K. Ramesh, G.S. Roopa, B.J. Gireesha, S.A. Shehzad, F.M. Abbasi, An electro magnetohydrodynamic flow of Maxwell nanoliquid past Riga Plate: a numerical study, J. Braz. Soc. Mech. Sci. Eng. 39 (2017) 4547-4554.

[20] J.C. Cuevas, F. J. García-Vidal, Radiative heat transfer, ACS Photonics. 5(10) (2018) 3896–3915.

[20] L.J. Fernández-Alcázar, H. Li, M.N.T. Kottos, Implementation of optimal thermal radiation pumps using adiabatically modulated photonic cavities, ACS Photonics. 8(10) (2021) 2973-2979.

[21] Y. Li, W. Li, T. Han, X. Zheng, J. Li, B. Li, S. Fan, C.W. Qiu, Transforming heat transfer with thermal metamaterials and devices, Nature Rev. Mat. 6 (6) (2021) 488-507.

[22] W.A. Callahan, D. Feng, Z.M. Zhang, E.S. Toberer, A.J. Ferguson, E.J. Tervo, Coupled charge and radiation transport processes in thermophotovoltaic and thermoradiative cells, Physical Rev. Appl. 15 (2021) 054035. https://doi.org/10.1103/PhysRevApplied.15.054035

[23] P.R. Stauffer, F. Rossetto, M. Leoncini, G.B. Gentilli, Radiation patterns of dual concentric conductor microstrip antennas for superficial hyperthermia, IEEE Transact. Biomed. Eng. 45(5) (1998) 605–613.

[24] J.H. Torres, M. Motamedi, A.J. Welch, 1990, Disparate absorption of argon laser radiation by fibrous verses fatty plaque: implications for laser angioplasty, Lasers in Surgery and Medicine. 10 (1990) 149–157.

[25] M. Rahimi-Gorji, C. Debbaut, G. Ghorbaniasl, S. Cosyns, W. Willaert, W. Ceelen, Optimization of intraperitoneal aerosolized drug delivery: A computational fluid dynamics (CFD) and experimental study, Scientific Reports. (2021).
https://doi.org/10.21203/rs.3.rs-1070871/v1

[26] M. Rahimi-Gorji, L.V. de Sande, C. Debbaut, G. Ghorbaniasl, H. Braet, S. Cosyns, K. Remaut, W. Willaert, W. Ceelen, Intraperitoneal aerosolized drug delivery: Technology, recent developments, and future outlook, Adv. Drug Delivery Rev. 160 (2020) 105-114.

[27] H. Braet, M. Rahimi-Gorji, C. Debbaut, G. Ghorbaniasl, T.V. Walleghem, S. Cornelis, S. Cosyns, C. Vervaet, W. Willaert, W. Ceelen, S. C. De Smedt, K. Remaut, Exploring high pressure nebulization of Pluronic F127 hydrogels for intraperitoneal drug delivery, European Journal of Pharmaceutics and Biopharmaceutics. 169 (2021) 134-143.

[28] M. Ramzan, M. Bilal, J.D. Chung, Radiative Williamson nanofluid flow over a convectively heated Riga plate with chemical reaction-A numerical approach, Chin J Phys. 55 (2017)1663-1673.

[29] S.R. Mishra, MD. Shamshuddin, O. Anwar Bég and A. Kadir, Viscous dissipation and Joule heating effects in non-Fourier MHD squeezing flow, heat and mass transfer between Riga plates with thermal radiation: variational parameter method solutions, Arabian J. Sci. Eng. 44 (2019) 8053–8066.

[30] M. Rooman, M.A. Jan, Z. Shah, P. Kumam, A. Alshehri, Entropy optimization and heat transfer analysis in MHD Williamson nanofluid flow over a vertical Riga plate with nonlinear thermal radiation, Scientific Reports.11 (2021) 18386.

[31] A. Shafiq, Z. Hammouch, A. Turab, Impact of radiation in a stagnation point flow of Walters' B fluid towards a Riga plate, Therm. Sci. Eng. Prog. 6 (2018) 27-33.

[32] N.A. Zainal, R. Nazar, K. Naganthran, I. Pop, Unsteady stagnation point flow past a permeable stretching/shrinking Riga plate in Al_2O_3-Cu/H_2O hybrid nanofluid with thermal radiation, Int. J. Numer. Methods for Heat & Fluid Flow. (2021).

[33] S.K. Rawat, A. Mishra, M. Kumar, Numerical study of thermal radiation and suction effects on copper and silver water nanofluids past a vertical Riga plate, Multidisc. Mod. Mat. Struc. 15(4) (2019) 714-736.

[34] P. Goldsmith, F.G. May, Diffusiophoresis and thermophoresis in water vapour systems, C.N. Davies (Ed.), Aerosol, Science, Academic Press, London (1966).

[35] S.L. Goren, Thermophoresis of aerosol particles in laminar boundary layer on flat plate, J. Colloid Interface Sci. 61 (1977) 77-85.

[36] L. Talbot, R.K. Cheng, R.W. Schefer, D.R. Willis, Thermophoresis of particles in a heated boundary layer, J. Fluid Mech. 101 (1980) 737-758.

[37] P. Ganesan, R.K. Suganthi, P. Loganathan, Thermophoresis particle deposition effects in a free convective doubly stratified medium over a vertical plate. Meccanica, 49 (2014) 659–672.

[38] K. Das, S. Jana, P.K. Kundu, Thermophoretic MHD slip flow over a permeable surface with variable fluid properties, Alex. Eng. J. 54 (2015) 35-44.

[39] J. Zueco, O. Anwar Bég, H.S. Takhar, V.R. Prasad, Thermophoretic hydromagnetic dissipative heat and mass transfer with lateral mass flux, heat source, Ohmic heating and thermal conductivity effects: network simulation numerical study, Appl. Therm. Eng. 29 (2009) 2808-2815.

[40] J.K. Madhukesh, S. Ravikumar, S. Varun Kumar R.J.P. Gowda, B.C. Prasannakumara, A. Sabir, A. Shehzad, Thermophoretic particle deposition and heat generation analysis of Newtonian nanofluid flow through magnetized Riga plate, Heat Transf. (2021).

[41] R.E. Abo-Elkhair, M.M. Bhatti, K.S. Mekheimer, Magnetic force effects on peristaltic transport of hybrid bio-nanofluid (Au-Cu nanoparticles) with moderate Reynolds number: An expanding horizon. International Communications in Heat and Mass Transfer. 2021; 123:105228. https;//doi.org/10.1016/j.icheatmasstransfer.2021.105228

[42] J. K. Madhukesh, A. Alhadhrami, R. Naveen Kumar, R.J.P. Gowda, B.C. Prasannakumara, R.S. Varun Kumar, Physical insights into the heat and mass transfer in Casson hybrid nanofluid flow induced by a Riga plate with thermophoretic particle deposition, Proc. IMchE, Part E: J. Proc. Mech. Eng. (2021). https://doi.org/10.1177/09544089211039305

[43] E.O. Fatunmbi, A.T. Adeosun, S.O. Salawu, Irreversibility analysis for Eyring-Powell nanoliquid flow past magnetized riga device with nonlinear thermal radiation, Fluids. 6(11) (2021) 416. https://doi.org/10.3390/fluids6110416.

[44] O. Anwar Bég, M.S. Khan, I. Karim, M.M. Alam, M. Ferdows, Explicit numerical study of unsteady hydromagnetic mixed convective nanofluid flow from an exponentially stretching sheet in porous media, Appl. Nanosci. 4(8) (2014) 943-957.

[45] M. K. Partha, P. V. S. N. Murthy, G. P. Rajasekhar, Effect of viscous dissipation on the mixed convection heat transfer from an exponentially stretching surface, Heat and Mass Transf. 41(4) (2005) 360–366.

[46] N. S. Akbar, D. Tripathi, Z. Khan, O. Anwar Bég, A numerical study of Magnetohydro-dynamic transport of nanofluids from a vertical stretching sheet with exponential temperature-dependent viscosity and buoyancy effects, Chem. Phys. Lett. 661 (2016) 20-30.

[47] MD. Shamshuddin, S.U. Khan, O. Anwar Bég, T.A. Bég, Hall current, viscous and Joule heating effects on steady radiative 3-D magneto-power-law polymer dynamics from an exponentially stretching sheet with power-law slip velocity: a numerical study, Therm. Sci. Eng. Prog. 20 (2020) 100732. https://doi.org/10.1016/j.tsep.2020.100732.

[48] M. Sajid, T. Hayat, Influence of thermal radiation on the boundary layer flow due to an exponentially stretching sheet, Int. Commun. Heat and Mass Transf. 35(3) (2008) 347–356.

[49] B. Bidin, R. Nazar, Numerical solution of the boundary layer flow over an exponentially stretching sheet with thermal radiation, Euro. J. Scientific Res. 33(4) (2009) 710–717.

[50] Y. Shagaiya, Z.A. Aziz, Z. Ismail, F. Salah, Double stratification effects on unsteady electrical MHD mixed convection flow of nanofluid with viscous dissipation and Joule heating, J. Appl. Res. Tech. 15 (2017) 464-476.

[51] W.N. Mutuku, O.D. Makinde, Double stratification effects on heat and mass transfer in unsteady MHD nanofluid flow over a flat surface, Asia Pacific J. Comput. Eng. 4 (2017) 2.https://doi.org/10.1186/s40540-017-0021-2

[52] E. Hairer, S. Nørsett, G. Wanner, Solving Ordinary Differential Equations- I: Non-stiff Problems, Second edition, Springer-Verlag, Berlin (1993).

[53] T. Hayat, M. Rashid, M. Imtiaz, A. Alsaedi, MHD effects on a thermo-solutal stratified nanofluid flow on an exponentially radiating stretching sheet, J. Appl. Mech. Tech. Phys. 58(2) (2017) 214-223.

[54] M.Z.H. Supian, N.A.A.M. Nasir, A. Ishak, Stagnation point flow and heat transfer over an exponentially stretching/Shrinking Riga Plate with effects of radiation and Heat source/sink, Magnetohydrodynamics, 57(3) (2021) 405-416.

[55] M.S. Alam, M.M. Rahman, M.A. Sattar, Transient magnetohydrodynamics free convective heat and mass transfer flow with thermophoresis past a radiate incline permeable plate in the presence of variable chemical reaction and temperature dependent viscosity, Nonlinear Analysis: Model Control 14(1) (2009) 3-20.

[56] P. Mathur, S.R. Mishra, Free convective magnetohydrodynamic flow over an exponentially stretching sheet with radiation, Heat Transf. 48(7) (2019) 3371-3383.

NOMENCLATURE

A	Riga plate electrode width parameter
a	constant
a_1	width of concentration of the solute [m]
b	constant
c	constant
C	concentration of the solute [$mol\ m^{-3}$]
C_f	skin friction coefficient
C_p	specific heat at constant pressure [$J\ Kg^{-1}K^{-1}$]
C_1	constant term
C_2	constant term
C_3	constant term
C_t	constant term
C_s	constant term
C_m	constant term
C_w	concentration at the stretching surface [$mol\ m^{-3}$]
C_∞	ambient concentration [$mol\ m^{-3}$]
d	constant
D_B	species mass diffusion [m^2 / s]
g	gravitational acceleration [m / s^2]

j_0 current density applied to electrode [A/m^2]
k_1 absorption factor [m^{-1}]
k^{th} thermophoretic coefficient
K_n Knudsen number
L reference length [m]
M modified Hartmann number
M_0 Plate surface magnetization [NA/m] Telsa
Nu Nusselt number
Pr Prandtl number
q_r Radiative heat flux [Wm^{-2}]
Q modified magnetic interaction number
Q_0 internal heat source/sink
R Radiation parameter
Re_x local Reynolds number
S heat source/sink parameter
Sc Schmidt number
Sh Sherwood number
St thermal stratification parameter
Sm solutal stratification parameter
T temperature of the field in the boundary layer [K]
T_w temperature at the stretching surface [K]
T_∞ ambient temperature [K]
u stretching velocity [m/s]
U_0 reference velocity [m/s]
v velocity component in y-direction [ms^{-1}]
x, y, z Cartesian coordinates

GREEK SYMBOLS

α thermal diffusivity [m^2/s]
β_0 thermal expansion coefficient [$1/K$]
υ kinematic viscosity [$m^2 s^{-1}$]
ρ density of base fluid [$kg\ m^{-3}$]
σ_1 Stefan-Boltzmann constant [$Wm^{-2}K^{-4}$]
λ mixed convection parameter
λ_g, λ_p fluid thermal conductivities [W/m/K]
τ thermophoretic parameter
θ dimensionless temperature
ϕ dimensionless concentration
η similarity variable
ψ stream function